Journal of Food Engineering 323 (2022) 110917

Contents lists available at ScienceDirect

Journal of Food Engineering

journal homepage: www.elsevier.com/locate/jfoodeng

Effect of temperature on rheological, structural, and textural properties of soy protein isolate pastes for 3D food printing

Jingwang Chen [a,b], Hongnan Sun [a,**], Taihua Mu [a,*], Christophe Blecker [c], Aurore Richel [d], Gaëtan Richard [b], Nicolas Jacquet [c], Eric Haubruge [b,***], Dorothée Goffin [b,****]

[a] Lab of Food Chemistry and Nutrition Science, Institute of Food Science and Technology, Chinese Academy of Agricultural Sciences, Key Laboratory of Agro-Products Processing, Ministry of Agriculture and Rural Affairs, No.2 Yuan Ming Yuan West Road, Haidian District, Beijing, 100193, China
[b] Smart Gastronomy Lab, Terra Research Center, University of Liege - Gembloux Agro-Bio Tech, Passage des Déportés, Gembloux, 5030, Belgium
[c] Laboratory of Food Science and Formulation, Faculty of Gembloux Agro-Bio Tech, University of Liège, Avenue de la Faculté 2-B, Gembloux, 5030, Belgium
[d] Laboratory of Biomass and Green Technologies, University of Liege-Gembloux Agro-Bio Tech, Passage des Déportés 2B, Gembloux, 5030, Belgium

ARTICLE INFO

Keywords:
Temperature
3D printing
Soy protein isolate
Rheology
Structure
Texture

ABSTRACT

Herein, we investigated the influence of temperature on the rheological properties, 3D printability, and textural characteristics of soy protein isolate (SPI) pastes. All protein pastes showed shear-thinning behavior and high temperature improved the storage modulus (G′), the yield stress (τ_y), and the minimum flow stress (τ_f) of SPI paste. However, the addition of sodium alginate and gelatin reduced G′, τ_y, and τ_f of SPI-based pastes. After adding gelatin, more stable 3D printed structures formed with higher hardness, resilience, cohesiveness, springiness, and chewiness at higher printing temperatures of 35 °C and 45 °C. The addition of gelatin and higher printing temperatures promoted the formation of tight connections between soy protein particles which induced the formation of a dense 3D structure in SPI-based pastes. Overall, this work provided useful information to prepare protein-based food with good 3D printability.

1. Introduction

Three-dimensional (3D) printing is a novel manufacturing technology using computer-designed digital model files and different raw materials to construct objects. More specifically, 3D food printing (3DFP) technology integrates 3D printing and digital cooking technologies to shape food products. This technology has convenient and flexible design which uses a relatively fast processing with high precision and quality at low production costs (Yang et al., 2017). Apart from customizing food shapes, 3DFP can also help to achieve personalized nutrition and energy design, which could meet consumers' needs for novel adapted food with a unique structure, texture, and nutrition (Sun et al., 2015). Some food ingredients can directly be used for 3D food printing without using additives, such as chocolate (Lanaro et al., 2017), cheese (Le Tohic et al., 2018), mashed potatoes (Liu et al., 2018a), starches (Guo et al., 2021), etc. On the other hand, some food materials, such as rice, meat, fruits, and vegetables, undergo some difficulties to be directly extruded (Lanaro et al., 2017). Therefore, starch, food hydrocolloids, enzymes, and other ingredients are often added to improve the printability and structural stability of food matrix to meet the requirements for 3D printing (Chen et al., 2019a; Du et al., 2021a; Severini et al., 2018; Wang et al., 2018; Yang et al., 2018; Zhao et al., 2020). 3D printability of food materials is related to their rheological properties and food matrix, which are widely investigated to predict the printing performance of food materials (Liu et al., 2018a, 2019b, 2020a; Zhu et al., 2019; Pérez et al., 2019).

Proteins constitute the important components of all living cells and tissues of the human body and participate in most biological functions. For people have difficulties in chewing, swallowing, or disliking protein-rich foods, personalized and high-quality 3D printed protein products can solve their problems. Protein pastes or gel systems have certain extrusion and molding properties, but their 3D printed products generally have poor accuracy and present low stability. Adding sodium alginate, xanthan gum, konjac gum, and other polysaccharides can improve

* Corresponding author.
** Corresponding author.
*** Corresponding author.
**** Corresponding author.
E-mail addresses: honey0329@163.com (H. Sun), mutaihua@126.com (T. Mu), e.haubruge@ulg.ac.be (E. Haubruge), dorothee.goffin@uliege.be (D. Goffin).

https://doi.org/10.1016/j.jfoodeng.2021.110917
Received 18 August 2021; Received in revised form 12 December 2021; Accepted 13 December 2021
Available online 5 January 2022

the rheological properties and 3D printability of the protein pastes (Chen et al., 2019b; Phuhongsung et al., 2020). Liu et al. (2019) optimized the formula of bovine protein concentrate and sodium caseinate that exhibited the best 3D printability and printing accuracy with a total protein content of 40–45%. Whey protein and konjac gum system could be accurately printed to design 3D food and the obtained shapes were significantly improved when the protein content exceeded 20% (Phuhongsung et al., 2020). Chen et al. (2021) investigated the rheological properties and the 3D printability of five types of protein mixtures with fruit and vegetable powder, and found the best printability in the mixture containing peanut protein.

Temperature is known to affect the rheological properties of food material and in turn is expected to influence the final 3D printability of the material. When the sample is more solid and has less fluidity, the influence of temperature on its 3D printability is more pronounced. For instance, the storage modulus (G′) and loss modulus (G″) were found different in higher content of dehydrated potato puree at 10 °C, and the best results of 3D printing were obtained at 10 °C for a lower content of dehydrated potato puree, but the best results of printing were obtained at 30 °C for higher levels of dehydrated potato puree (Martínez-Monzó et al., 2019). The G′, flow stress (τ_f), and yield stress (τ_y) displayed a first increasing then decreasing when printing temperature increased from 65 °C to 85 °C with different concentrations of corn and rice starch (Zeng et al., 2020). With the increase of the 3D printing temperature, the sufficient chain interactions between starch particles led to the formation of a uniform gel structure with higher G′, τ_f, and τ_y, which in turn promoted the 3D printing performance (Liu et al., 2020a, b).

However, there are few studies on the effect of the temperature on the 3D printed protein-based objects. Therefore, the aim of the present study is to investigate the effect of temperature on the rheological properties of soy protein isolate-based pastes, and evaluate the structural and textural characteristics of 3D printed objects that formed by soy protein isolate-based pastes at different printing temperatures. The corresponding results could provide us with fundamental mechanisms to build up a better understanding of the impact of the printing temperature on the 3D printing feasibility and printed structure stability for soy protein isolate-based pastes.

2. Materials and methods

2.1. Materials

Soy protein isolate (SPI, ProFam-974) was donated by Archer Daniels Midland Company (ADM, Decatur, IL, USA) with the protein content of 92.1% (dry basis). The food-grade sodium alginate and gelatin (type A, Mw 40,000–50,000 Da) were purchased from Henan Zhongxin Chemical Co., Ltd. (Zhengzhou, Henan, China) and Atlas Ltd. (Harelbeke, West Flanders, Belgium), the bloom index of gelatin was 180. Ethanol and glutaraldehyde were of analytical grade.

2.2. Sample preparation

The SPI-based pastes with or without gelatin and sodium alginate were prepared according to the previous method (Chen et al., 2019b). We had tested different SPI concentrations to form the paste and to extrude it out, the 20% (w/v) SPI paste was suitable to form the 3D structure after extruding it out from the nozzle. The protein paste with 2% gelatin could form a weaker gel at 35 °C and the protein paste with 6% gelatin could form a harder gel. Therefore, two concentrations of gelatin were chosen to study the effect of temperature on the 3D printing behavior of protein pastes. Briefly, 0.5 g sodium alginate was well dissolved in 100 mL of deionized water under continuous stirring for 2 h until complete dissolution. Then, 2 and 6 g gelatin were added to the sodium alginate solution, and incubated at 45 °C by magnetic stirring (IKA RCT basic, Germany) until the complete dissolution. Afterwards, 20 g SPI was added to the solution and mixed using a glass rod until the complete disappearance of powder aggregates. A SPI paste with a concentration of 20% (w/v) SPI was used as a control and was prepared through an accurate mixing of the required SPI powder with deionized water using a glass rod. The protein pastes with 0.5% sodium alginate, and 2% and 6% (w/v) gelatin were named SAG-2 and SAG-6, while the control was named S. All the pastes were stored in a fridge (BMGN2450II, Infrico., Belgium) at 4 °C overnight and heated to the printing temperature before testing or 3D printing while all samples preparation were carried out at room temperature.

2.3. Rheological properties

Rheological properties of the protein pastes were determined by a rheometer (MCR 302, Anton Paar, Austria) using a stainless steel parallel plate with a diameter of 50 mm and a 1.0 mm gap. The flow sweeps were carried out for shear stress and viscosity with shear rates ranging from 0.01 to 10 s^{-1}. The dynamic viscoelastic properties were evaluated by the oscillatory frequency sweep from 0.01 to 100 rad/s at a constant strain of 0.5%, and the storage modulus (G′), loss modulus (G″) and loss tangent (tan δ) were recorded. The strain sweep experiments were carried out at 1 Hz in a range of 0.01–100 for strain (γ) in the oscillation mode. The minimum flow stress (τ_f) to get a flow corresponds to shear stress where the G′ is equal to G″, and the yield stress (τ_y) is the stress point where G′ decreased by 3% (Liu et al., 2020b). Before the test, the excess paste was eliminated and light silicon oil was applied to reduce the evaporation, and the samples were equilibrated for 5.0 min to get a steady-state (Liu et al., 2018a). From the view of experimental environment, edible condition and sample preparation, different temperatures namely 25, 35, and 45 °C were applied for the measurements. The 25 °C is around the room temperature, the 35 °C is around the body temperature (~37 °C), and the 45 °C is temperature to solve the gelatin during the protein paste preparation. The software of Rheoplus/32 v3.21 (Anton Paar Germany Gmbh, Germany) was used to analyze the rheological data.

2.4. 3D printing process

An extrusion-based 3D printer 3.0 developed by Felix Co. Ltd., Netherlands was used. Readers could find the detailed information of this 3D printer and relevant information from our previous publication (Chen et al., 2019b). The nozzle diameter is 1.55 mm, and the printing parameters include a nozzle height of 1.0 mm, a shell thickness of 1.55 mm, a printing speed of 10 mm/s, a layer height of 0.6 mm, a flow rate of 80%. The pastes were preheated to the printing temperature and then transferred into the syringe carefully without bringing in air bubbles. Based on a premade electronic model, different protein pastes were extruded to form hollow cylinders (diameter × height: 25 × 20 mm) at 25, 35 and 45 °C. The printing process and the results were recorded by camera (EOS 750D, Canon, Japan) to check the changes in appearance of the objects at different times and their shape stability. During the printing process, the camera was placed ~15 cm away from the printing platform, and the height was ~8 cm based on the printing platform. The camera lens was tilted about 60° toward the printer during printing. The side profile and top profile of the 3D printed sample were captured when the distance between the camera lens was facing the side and the top of the 3D printed sample was ~8 cm. The indoor normal incandescent light was used to take pictures. The solid cylinders were printed with the same parameters, the bottom layer thickness was 0.1 mm and the fill density was 100%. The CURA 15.04.6 software (Ultimaker B·V., The Netherlands) was used to control the 3D printing tests and the printing temperatures. The printed objects were directly covered to avoid dehydration by aluminum specimen boxes, and stored in the refrigerator (4 °C) until the following measurements.

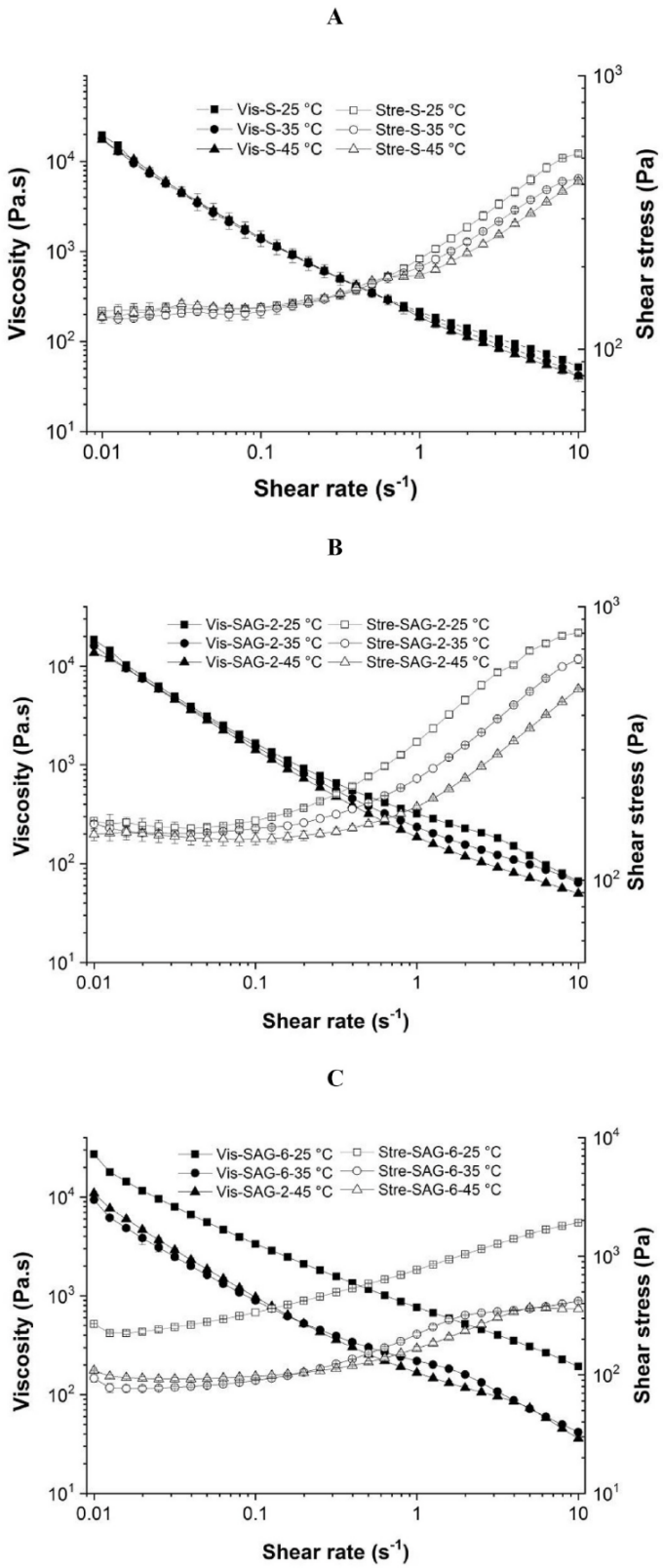

Fig. 1. Changes in shear stress and viscosity of S (A), SAG-2(B), and SAG-6 (C) as a function of shear rate from 0.01 to 10 s^{-1} at 25, 35, and 45 °C.

2.5. Microstructure

Scanning electron microscopy (SEM) was performed to examine the structural characteristics of printed solid cylindrical samples. The center parts of the printed solid cylinders were cut into cubes (with length around ~1–2 mm), which were fixed with 2.5% (v/v) glutaraldehyde in 0.1 M phosphate buffer (pH 6.8) for 24 h. Then the cubes were dehydrated in ethanol solutions with a serial concentration of 50, 70, 90, and 100% (v/v), and finally dried by nitrogen blowing (Wang et al., 2018). The dried samples were sputter-coated with gold for 30 s with a Baltek platinum coater and then examined using a scanning electron microscope (Quanta 600, Quanta System, Italy) at an acceleration voltage of 10 kV.

2.6. Textural properties

A texture analyzer with an acrylic cylindrical plate of 35 mm diameter (TA-XT2i, Stable Micro-Systems Ltd, UK) was used to analyze the textural properties of 3D printed solid cylinders. The testing speed was 1.0 mm/s, the sample's height was compressed to 25% by a load cell of 50 kg with trigger force of 5 N, and then the sample was decompressed. After an interval of 5 s, this compression-decompression cycle was repeated. The textural properties experiment was carried out in triplicates in sealed containers with a constant temperature of 4 °C.

2.7. Statistical analysis

All experiments were carried out at least in triplicates. All data were analyzed by SPSS software for Windows (Version 18.0, SPSS Inc., Chicago, IL, USA), and the results were expressed as mean ± standard deviations. The curves were made by Originpro (2019) software (Originlab, Northampton, MA, USA). ANOVA and the Duncan's new multiple range tests were performed to establish significance among mean values at a confidence level of 95%.

3. Results and discussion

3.1. Rheological properties

3.1.1. Steady flow behavior

The apparent viscosity of food material is directly influenced by its composition and in the case of 3D printing. The ideal formula could display a suitable viscosity that should be low enough to extrude out of the nozzle, and high enough to support the combined layers (Liu et al., 2018b). Flow curves at different temperatures for SPI-based pastes are shown in Fig. 1. An increase in shear stress and a decrease in viscosity were observed with the shear rate increasing from 0.01 to 10 s^{-1} at 25, 35, and 45 °C, suggesting that all the samples showed shear-thinning behavior. These materials thus show a potential to be printable, namely extrudability out of the nozzle and self-supportive as the shear thinning behavior is very important in this case (Lipton, 2017).

The effect of temperature on the shear stress and viscosity of SAG-2 and SAG-6 was more obvious than S. The viscosities of S at 25, 35 and 45 °C were similar when the shear rate was lower 10 s^{-1}. However, for the SAG-2, when shear rate was higher than 0.3 s^{-1}, the viscosity at 25 °C was higher than that at 35 °C and 45 °C. Due to the fact that gelatin gets easily melted at higher temperatures, it leads to the reduction of pastes' viscosity. At 25 °C, an increase in the gelatin content (2% and 6%) resulted in a general increase in apparent viscosity of the protein pastes (Fig. 1). The protein pastes with 6% gelatin exhibited the highest viscosity and shear stress compared to other pastes. The addition of κ-carrageenan and starch also led to an increase in the viscosity and shear stress of mashed potatoes (Liu et al., 2018b, 2018c). However, with temperature increase to 35 °C and 45 °C, the viscosity and shear stress of SAG-2 and SAG-6 were significantly reduced ($p < 0.05$; Fig. 1B and C), and the SAG-6 showed the lowest viscosity and shear stress at 45 °C (Fig. 1C), while the SAG-2 showed the highest viscosity at 25 °C when the shear rate was 10 s^{-1} (Fig. 1B). Similarly, the viscosity of potato puree at 30 °C was also lower than that at 10 and 20 °C as a function of shear rate from 10 to 100 s^{-1} (Martínez-Monzó et al., 2019). Gelatin can absorb large amounts of water and then be dissolved in warm water (~40 °C) when the flexible single random coils are formed

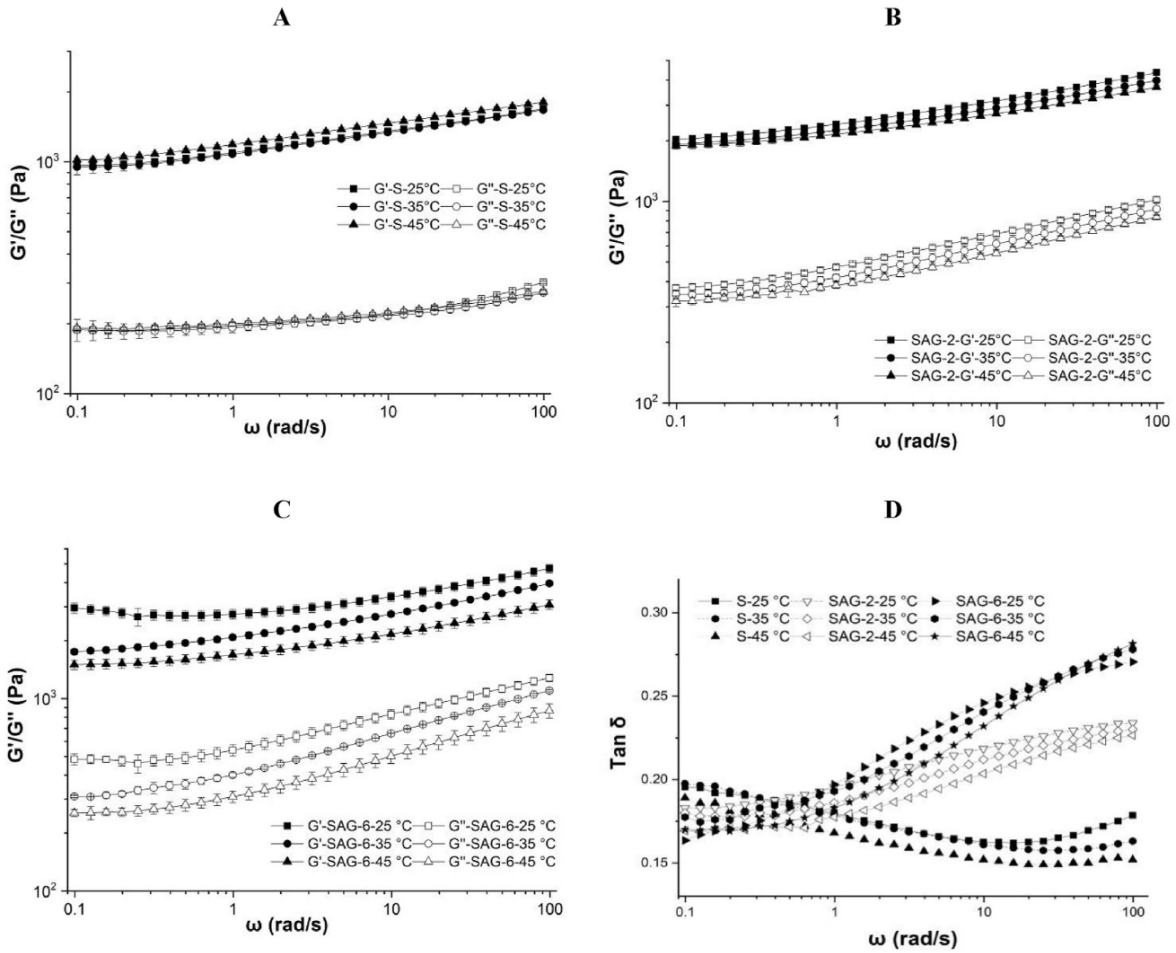

Fig. 2. Storage modulus (G′), loss modulus (G″) and tan σ (tan δ = G″/G′) for S, SAG-2, and SAG-6 at 25, 35, and 45 °C as a function of frequency from 0.1 to 100 rad/s with a constant strain of 0.5%. A, B and C: G′ and G″ for S, SAG-2, and SAG-6; D: tan δ for S, SAG-2, and SAG-6.

in the hydrated particles (Godoi et al., 2016). Lower temperature contributed to a consistent food structure. While cooling to room temperature, gelation could occur due to some of the segments of polypeptide chains of gelatin which were connected to form junction zones with triple-helix-like structures in collagen (Godoi et al., 2016). This procedure led to an increase in the viscosity of SAG-2 and SAG-6. Besides, some soy protein particles might be entrapped inside gelatin network and the new formed structure could not be disrupted at a shear rate ranging from 0.1 to 10 s^{-1}.

3.1.2. Dynamic viscoelasticity

The storage modulus (G′) and loss modulus (G″) are often used as indicators to evaluate the elasticity and viscosity behavior of samples and reflect their mechanical strength. The G′, G″ and loss tangent (tan δ) versus log frequency curves for different protein pastes at various temperatures are shown in Fig. 2. With an increase of angular frequency, the G′ and G″ of S, SAG-2, and SAG-6 increased at 25, 35, and 45 °C, respectively. The G′ of S at 45 °C was higher than that at 25 and 35 °C, which indicates that the soy protein particles might absorb more water and could form a stronger structure at a higher temperature. Moreover, the addition of gelatin significantly affected the mechanical strength of protein paste at different temperatures. The G′ and G″ of protein pastes with gelatin obviously decreased when temperature increased to 35 and 45 °C. The G′ for SAG-2 and SAG-6 at 25 °C (2975 and 3190 Pa) were higher than that at 35 °C (2750 and 2580 Pa) and 45 °C (2585 and 2045 Pa) at a frequency of 6.28 rad/s and similar results were found concerning the evolution of the viscosity (Fig. 1). For the protein pastes with gelatin, some soy protein might be easily trapped inside the gelatin network together with water during the paste preparation and heat treatment (35 and 45 °C), which could allow the formation of a stronger gel structure with higher G′ at 25 °C (Fig. 2B and C). The samples with higher G′ and yield stress could form stable 3D printed structure with a better shape retention (Costakis et al., 2016; Liu et al., 2018c). An increase of the printing temperature led to a decrease of G′ and G″, which is useful for the formation of stable 3D printed structure (Martínez-Monzó et al., 2019).

For all samples, the G′ was higher than G″ and tan δ was less than 1.0, which indicates that these samples display gel-like characteristics with a dominant elastic behavior (Yang et al., 2018). The tan δ at various temperatures gradually increased with an increasing frequency for SAG-2 and SAG-6, but reduced for S (Fig. 2D). The tan δ for S was higher than that for other samples when the frequency was below 0.5 rad/s, while when the frequency exceeded 1.0 rad/s, the tan δ for SAG-2 and SAG-6 at different frequencies significantly increased compared to those of S at 25, 35, and 45 °C (Fig. 2D). The SAG-6 had the highest tan δ at 100 rad/s namely 0.228, 0.272, and 0.245 at 25, 35, and 45 °C, respectively. The tan δ for SAG-6 at 35 and 45 °C were higher than that at 25 °C when the angle frequency passed 40 rad/s, but tan δ for S and SAG-2 at 35 and 45 °C were still lower than that at 25 °C. At 35 and 45 °C, the protein pastes with gelatin showed fluid-like flow properties at higher frequencies, which indicates that the thermal treatment could increase the viscosity ratio of the protein pastes. Addition of gelatin enhanced G′ and G″ of protein paste at 25 °C as well as the viscosity and stress values, which indicates that a more stable structure was formed as temperature decreased (Liu et al., 2018b, 2020a; Martínez-Monzó et al., 2019).

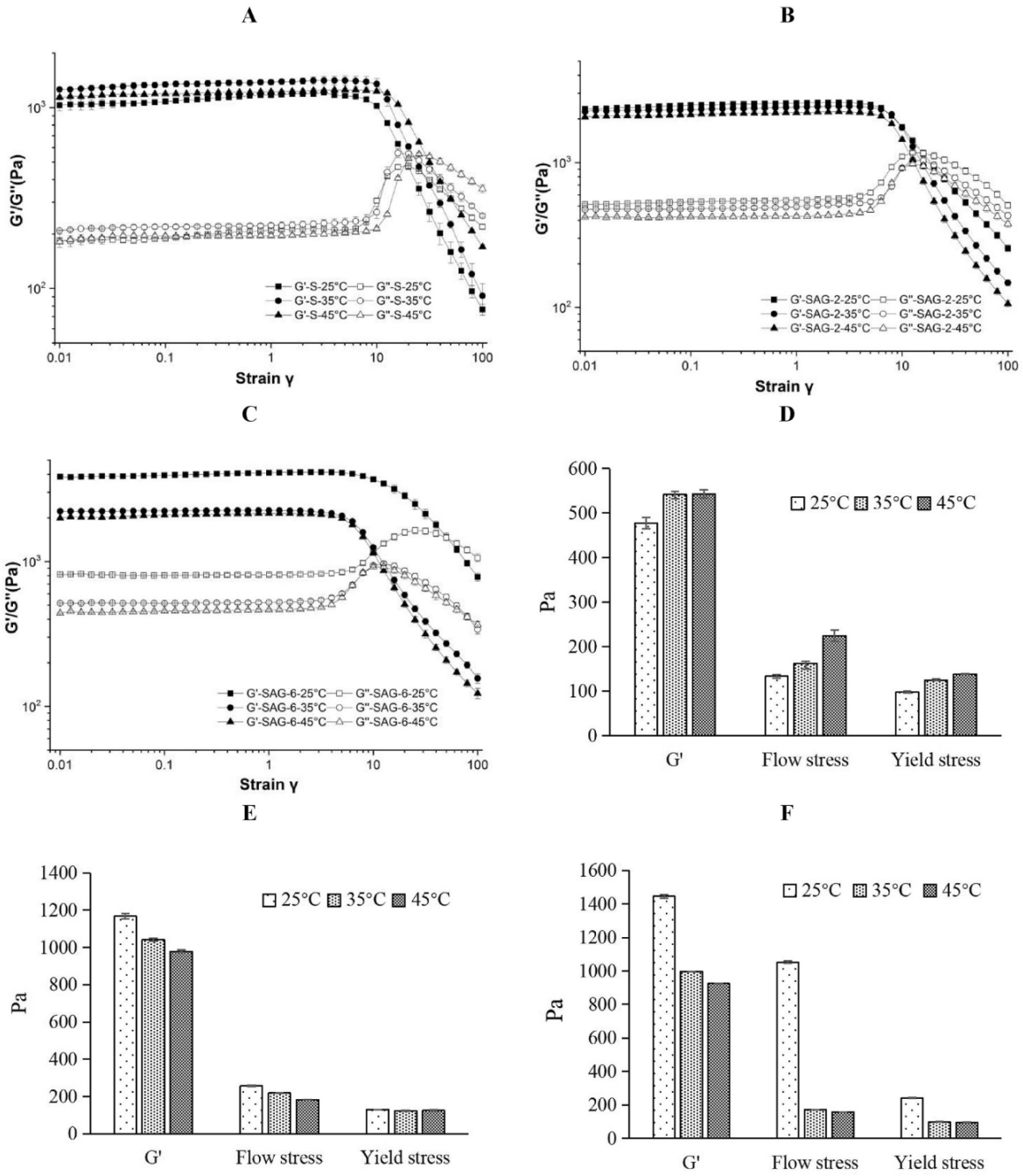

Fig. 3. Strain sweep test for S, SAG-2, and SAG-6 at 25, 35, and 45 °C. A, B and C: strain sweep for S, SAG-2, and SAG-6 at 25, 35, and 45 °C; D, E and F were the storage modulus (G′) at cross point, flow stress (τ_f), and yield stress (τ_y) for S, SAG-2, and SAG-6 at 25, 35, and 45 °C.

3.1.3. Stress sweep

Strain sweep results for SPI-based pastes at different temperatures are shown in Fig. 3. The G′ at cross point, flow stress (τ_f), and yield stress (τ_y) of S, SAG-2, and SAG-6 were mainly dependent on temperature (25, 35 and 45 °C). At lower strain, the G′ and G″ kept at a constant value for different temperatures, but G′ decreased and G″ increased significantly when the strain exceeded 10%. In addition, the curves of G′ and G″ cross each other when strain increased further (Fig. 3A, B, and C). Similar results were also found for the konjac gel with different concentrations of whey protein (5–30%) (Du et al., 2021b). For S, when temperature increased from 25 to 45 °C, the G′ at cross point increased from 477.60 to 543.30 Pa, τ_f increased from 133.30 to 224.60 Pa, and τ_y increased from 98.19 to 138.90 Pa (Fig. 3D). More water was absorbed by SPI when temperature increased which might also lead to the mechanical strength increase and a better 3D printing performance. However, for SAG-2 and SAG-6, G′, τ_f, and τ_y were reduced significantly with temperature increase (Fig. 3E and F), especially for SAG-6, whereby G′ decreased from 1445.00 to 925.3 Pa, τ_f decreased from 1052.00 to 156.50 Pa, and τ_y decreased from 240.50 to 95.00 Pa (Fig. 3F). The reduction in τ_f indicates that the sample presents a better flow ability and therefore a lower minimum pressure is required to extrude it out of the nozzle (Liu et al., 2020b). The SAG-6 at 35 and 45 °C could thus be easily extruded out of the nozzle, allowed to build up a stable 3D structure at room temperature (~25 °C) due to its rapid reforming ability at lower shear strains. However, the SAG-6 might be hard to be extruded out of the nozzle directly to form a precious 3D structure at a printing temperature of lower than 25 °C. The τ_f and τ_y for the SAG-2 at 25 °C were lower than that of SAG-6, which allowed it to flow easily even at 25 °C (Fig. 3E). These findings are in agreement with the results on 3D printability and stability of protein pastes at different

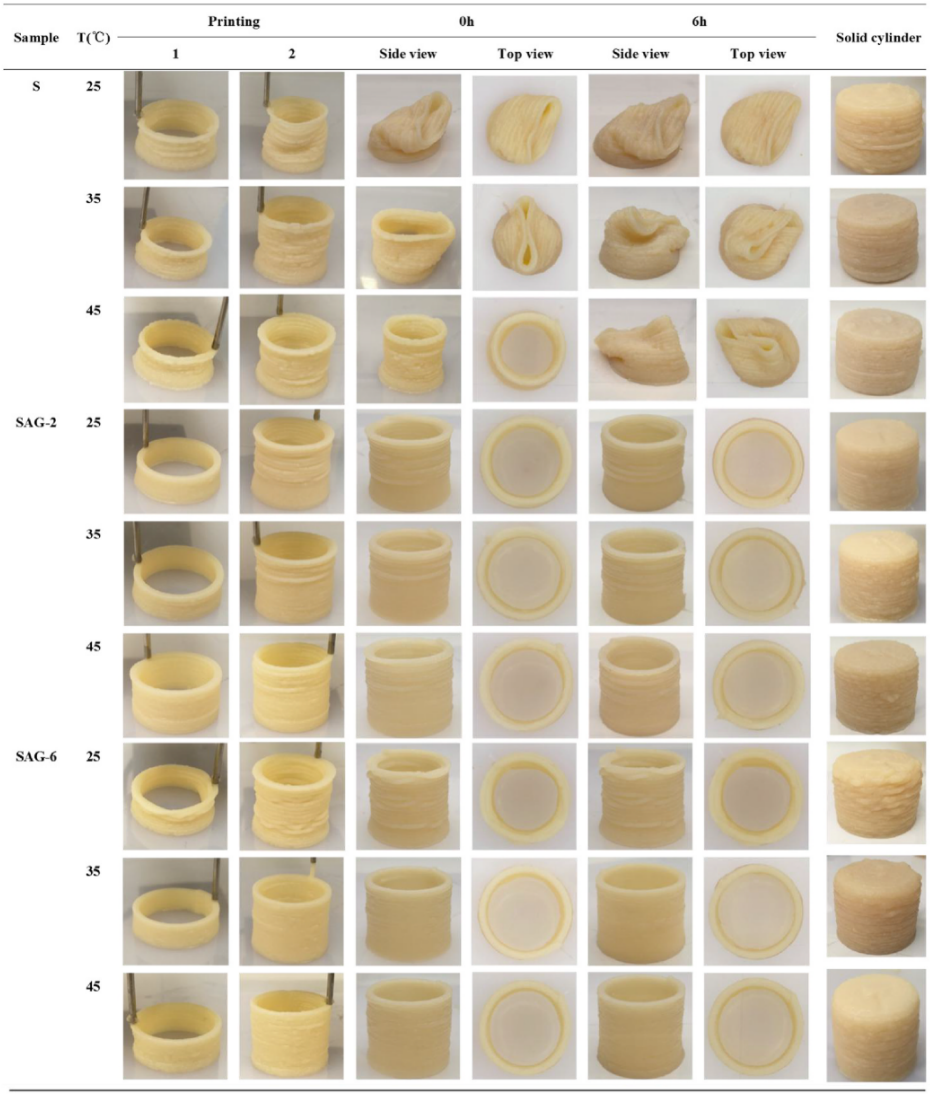

Fig. 4. The 3D printing behavior (printing 1 and 2) and stability (0 h and 6 h) of the printed cylinders (25 × 25 × 20 mm) with various SPI pastes at 25, 35, and 45 °C.

temperatures (Fig. 4). The mashed potato was also found to be easily extruded out at a higher temperature because of its low G′ and τ_y (Liu et al., 2020a).

3.2. Printability and stability

The printability of protein pastes and the stability of their corresponding 3D printed objects were evaluated by the observation of their printing behavior at different time (Fig. 4, printing 1 and 2) and the performance of 3D printed objects after printing 0 and 6 h (Figs. 4 and 0 h and 6 h). As observed during the printing process, S was extruded out at 25, 35 and 45 °C owing to its low viscosity (Fig. 1A). At 25 and 35 °C, S could be used to build up the designed shape through the deposit of successive layers during the beginning of the printing process (Fig. 4, printing 1). However, when the object height exceeds ~10 mm, the cylindrical inner wall formed by deposition of the newly extruded material began to deform and this deformation gradually amplified as 3D printing process continued (Fig. 4, printing 2). The hollow cylinder of S remained stable for a while after printing, and then completely collapsed. The hollow cylinder of S could be printed at a printing temperature of 45 °C and stood for approximately 1 h, and then deformed completely. The solid cylinders of S were printed successfully at higher temperature, but still have printing defects of sagging and buckling after their storage at room temperature. The main reason might be that the mechanical strength of the S was too low to support the designed geometry which led to the complete collapse of the hollow cylinder (Liu et al., 2018b; Pulatsu et al., 2020).

After adding sodium alginate and gelatin, the mechanical strength of all the protein pastes and the structural stability of their corresponding 3D printed objects were significantly improved. The SAG-2 could be smoothly extruded out of the nozzle and be deposited layer after layer with high cohesion at 25, 35, and 45 °C. The corresponding 3D printed cylinders were stable and no collapse was observed after storage at room temperature for 6 h. At 25 °C, the SAG-6 was difficult to be extrude out, the filaments of its printed object was coarse and the SPI particles became visible which is similar with the milk protein gels printed filaments with higher protein content (500 g/L) (Liu et al., 2019a). Furthermore, weak cohesion could was found between the SAG-6 layers led to a low printing accuracy. At higher printing temperature, the sample could be extruded out easily and form an accurate and stable 3D printed structure due to its low viscosity at 35 and 45 °C and high G′ at 25 °C.

As the gelatin content increased, a gradual improvement of the visual quality and the stability of 3D printed objects was observed (Fig. 4). This is mainly because an increase in the gelatin content that led to an increase in G′ and viscosity for the protein pastes (25 °C). The addition of 2% of gelatin could be used to print objects and to improve the structure stability at room temperature. The addition of 6% of gelatin could

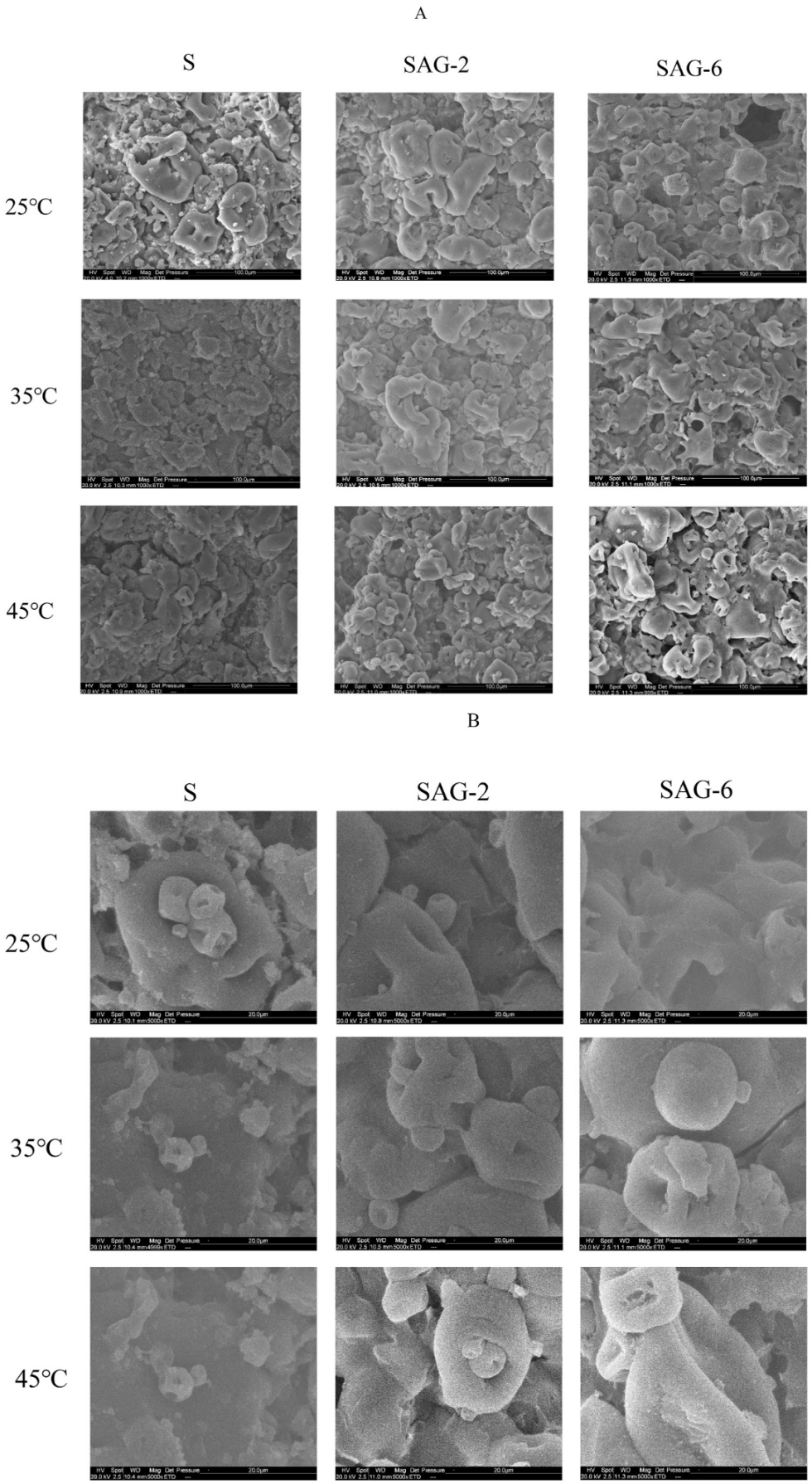

Fig. 5. SEM micrographs cross-section of 3D printed solid cylinders (25 × 25 × 20 mm) of SPI pastes at 25, 35, and 45 °C for S, SAG-2 and SAG-6 with magnification of 1000 (A) and 5000 (B).

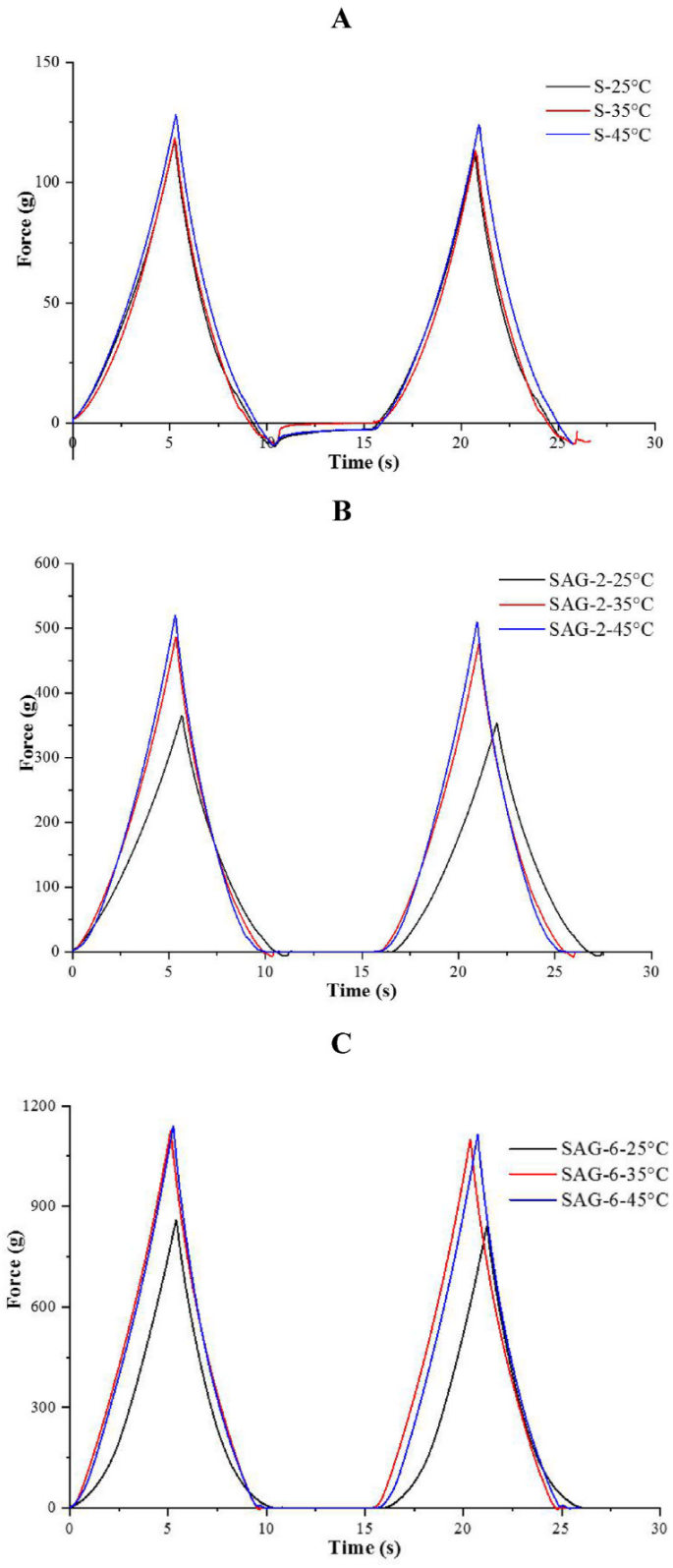

Fig. 6. Texture profiles analysis (TPA) of 3D printed solid cylinders (25 × 25 × 20 mm) of SPI pastes at 25, 35, and 45 °C for S (A), SAG-2 (B) and SAG-6 (C).

improve the printing behavior as well as the printed object's appearance at 35 °C and 45 °C. All these pastes allowed to print a solid cylinder at different temperatures, however, the printing accuracy was obviously influenced by the printing temperature and the formula. Indeed, the addition of gelatin improved the flowing ability of protein pastes at higher temperatures (35 °C and 45 °C) and enhanced their self-supporting ability at lower temperature (25 °C). Higher temperature led to the modification of fundamental rheological parameters (Fig. 3), which allowed the protein pastes to become more flowable, extrudable, and form 3D designed structure at room temperature. The method of modulating printing temperature was found helpful to improve the accuracy and the stability of 3D printed objects (Liu et al., 2020b).

3.3. Microstructure

Fig. 5 shows the SEM of 3D printed cylinder made of S, SAG-2, and SAG-6 pastes at different printing temperatures. It can be seen that the compactness of the printed 3D objects varied with printing temperature and the matrix used. The cross-section of the 3D printed object made of S at 25 °C was rougher than that at 35 and 45 °C. This might be attributed to the weak interaction between protein particles at 25 °C and only dependent on hydrogen bonding and the protein particles which were easier to disperse. The addition of sodium alginate and gelatin improved the cross-section structure of the printed object, and the 3D printed objects became more compact and smoother (Fig. 5A). There was a large pore in the micrographs of the SAG-6 paste printed at 25 °C, which was due to the high mechanical strength of the SAG-6 paste at 25 °C. Higher mechanical strength and too high viscosity at 25 °C for SAG-6 paste led to a weak bonding of between layers so that large pores were not observed at 35 °C and 45 °C. Fig. 5B shows the micrographs with higher magnification in which the protein particles in cylinder made of S were in a relatively loose state. However, the inter-molecular binding between the protein particles in SAG-2 was relatively tight and a layer of gelatin film was formed around the interconnected protein particles. In SAG-6, the binding between the protein particles became tighter with a high concentration of gelatin. According to previous results, the melting temperature of gelatin is around 28 °C. Therefore, with an increase of gelatin content in the protein pastes, the sample displays a softer performance and can easily pass through a syringe nozzle at higher temperature (Chen et al., 2019b). The gelatin formed a stable 3D network and entrapped the protein particles at 35 °C and 45 °C to form a relatively stable 3D structure when the temperature reached room temperature (around 25 °C). The starch gel displayed a porous network structure and the pores became thinner, shallower, and smaller with the temperature increase from 65 to 85 °C because of the gradual starch gelatinization (Zeng et al., 2021). Considering these results, the printing temperature highly influences the process of extruding and the formation of a compact protein network structure.

3.4. Textural characteristics

Fig. 6 shows the textural profiles of 3D printed solid cylinders after two compression-decompression cycles. The printing temperature significantly influenced the force profiles of the 3D printed protein solid cylinders of different protein pastes. The first peak indicates the hardness of samples and the addition of gelatin and sodium alginate increases the force peak of protein pastes. The relevant texture profiles analysis (TPA) was carried out for the 3D printed solid cylinders with different protein formulas at different printing temperatures (Table 1). At all printing temperatures, the SAG-2 and SAG-6 formed more stable 3D printed solid cylinders than S with higher hardness, resilience, cohesiveness, springiness, gumminess, and chewiness. The binding of protein and water, and the grid structure of protein molecules influenced the textural properties of protein pastes. It can thus be concluded that the textural property of 3D printed protein pastes solid cylinders are mainly dependent on their gelatin contents (Chen et al., 2019b). Similarly, the addition of higher concentrations of whey protein also enhanced the textural indicators of the konjac hybrid gel system (Du et al., 2021b).

The printing temperature significantly affected the textural properties of the samples. Generally, with printing temperature increasing, the hardness and chewiness of the objects made of S, SAG-2, and SAG-6 increased significantly, while the adhesiveness for S and SAG-2

Table 1
Texture profile analysis (TPA) indicators for different 3D printed solid cylinders of SPI pastes at different printing temperatures.

Sample	Temperature (°C)	Hardness (g)	Adhesiveness (g.s)	Resilience (%)	Cohesiveness –	Springiness (%)	Gumminess –	Chewiness –
S	25	120.20 ± 4.24^{b}	−32.35 ± 7.88^{a}	67.85 ± 0.25^{c}	0.91 ± 0.00^{a}	94.40 ± 1.03^{b}	109.24 ± 3.89^{b}	103.10 ± 2.55^{b}
	35	118.58 ± 10.51^{b}	−30.73 ± 7.45^{a}	69.81 ± 0.54^{b}	0.91 ± 0.01^{a}	95.27 ± 4.32^{b}	108.44 ± 10.92^{b}	103.08 ± 5.72^{b}
	45	126.61 ± 3.69^{a}	−21.65 ± 6.55^{b}	71.91 ± 0.42^{a}	0.92 ± 0.01^{a}	96.22 ± 3.35^{a}	116.55 ± 3.21^{a}	112.07 ± 1.36^{a}
SAG-2	25	348.45 ± 19.07^{c}	−2.87 ± 0.63^{a}	76.09 ± 0.54^{a}	0.92 ± 0.00^{b}	95.53 ± 1.17^{b}	322.14 ± 16.42^{c}	307.86 ± 19.13^{c}
	35	456.49 ± 28.45^{b}	−0.91 ± 1.01^{b}	74.42 ± 1.44^{a}	0.94 ± 0.00^{a}	98.37 ± 0.43^{a}	429.30 ± 28.31^{b}	422.34 ± 28.98^{b}
	45	518.48 ± 25.01^{a}	−0.02 ± 0.02^{b}	74.14 ± 0.91^{a}	0.94 ± 0.00^{a}	98.15 ± 0.46 ^{a}	487.75 ± 22.56^{a}	478.77 ± 22.92^{a}
SAG-6	25	856.65 ± 4.45 ^{b}	0.00 ± 0.00 ^{a}	78.42 ± 0.58 ^{a}	0.94 ± 0.00^{a}	99.06 ± 1.07 ^{a}	804.76 ± 0.64 ^{c}	797.16 ± 9.78 ^{c}
	35	1086.02 ± 30.67^{a}	0.00 ± 0.00 ^{a}	78.13 ± 0.86 ^{a}	0.94 ± 0.00^{a}	98.26 ± 0.37^{a}	1025.52 ± 27.16^{b}	1007.60 ± 26.01^{b}
	45	1128.69 ± 18.97^{a}	0.00 ± 0.00 ^{a}	75.99 ± 2.87 ^{a}	0.95 ± 0.01^{a}	98.01 ± 0.84^{a}	1072.66 ± 17.62^{a}	1051.33 ± 19.65^{a}

decreased. The resilience and springiness of 3D printed cylinders for S significantly increased ($p < 0.05$) from 67.85 ± 0.25% and 94.40 ± 1.03% at 25 °C to 71.91 ± 0.42% and 96.22% ± 3.35% at 45 °C, while there was no significant difference in springiness for S at 25 and 35 °C. A decrease of adhesiveness and an increase of hardness, gumminess, and chewiness was noticed for the 3D printed cylinder of S at 45 °C compared to that at 25 °C and 35 °C. After adding 0.5% of sodium alginate and 2% of gelatin, the printing temperature had a great influence on the texture index of the printed cylinders. As printing temperature increased from 25 °C to 45 °C, the hardness, resilience, gumminess, and chewiness of the 3D printed SAG-2 cylinders significantly increased, which indicates that sodium alginate and gelatin can be considered good additives for 3D printing of soy protein at a higher temperature. The printing temperature showed a little effect on the adhesiveness, resilience, cohesiveness, and springiness of the 3D printed SAG-6 cylinders (Table 1). However, the hardness and chewiness increased significantly at 35 and 45 °C as more protein particles might be entrapped in the 3D network of gelatin. Additionally, more compact network could be formed as sample's temperature decreased to room temperature for SAG-2 and SAG-6 (Fig. 5). It can be deduced that the textural properties of 3D printed solid cylinders made of protein paste were mainly dependent on the presence of gelatin than the SPI when the gelatin content exceeded 2%. More so, the textural variation of 3D printed solid cylinders made of protein pastes were consistent with the variation of mechanical strength (G′) for the protein pastes at 25, 35 and 45 °C (Fig. 2A and B).

4. Conclusion

The present study investigated the effect of temperature on the rheological properties, printability of SPI-based pastes, and the structural and textural properties of the corresponding 3D printed objects. For SPI pastes with lower gelatin content (SAG-2), the temperature had less impact on G′, τ_y and τ_f than for S and SAG-6. The SAG-2 displayed good extrusion ability and could form a stable 3D structure at 25, 35 and 45 °C. The SAG-6 exhibited lower viscosity, G′, τ_y, and τ_f at 35 and 45 °C which rendered it to be easily extruded out of the nozzle and form accurate and stable 3D printed cylinders as paste temperature decreased to room temperature (~25 °C). The 3D printability of protein pastes with different formulations was obviously improved by adjusting the printing temperature. The effect of the printing temperature on the microstructure and texture of 3D printed protein pastes cylinders varied greatly according to the gelatin content. These new findings provide basic information for the production of 3D printed protein-based food with a stable structure and good performance. Therefore, the optimization of the 3D printed food formula should coordinate with printing temperature to obtain stable 3D printed structures with high resolution and excellent accuracy. In addition, the influence of storage temperature on 3D printing products should also be considered.

Credit author statement

Jingwang Chen: Conceptualization, Methodology, Writing – original draft. Hongnan Sun: Writing – review & editing. Taihua Mu: Supervision, Project administration. Christophe Blecker: Investigation. Aurore Richel: Writing – review & editing. Gaëtan Richard: Investigation. Nicolas Jacquet: Investigation. Eric Haubruge: Funding acquisition. Dorothée Goffin: Writing – review & editing, Project administration

Declaration of competing interest

The authors declare that they have no known competing financial interests or personal relationships that could have appeared to influence the work reported in this paper.

Acknowledgement

The authors acknowledge the financial support from the Science and Technology Innovation Project of Chinese Academy of Agricultural Sciences and the fund of China Scholarship Council that enables us to carry out this study.

References

Chen, H., Xie, F., Chen, L., Zheng, B., 2019a. Effect of rheological properties of potato, rice and corn starches on their hot-extrusion 3D printing behaviors. J. Food Eng. 244, 150–158. https://doi.org/10.1016/j.jfoodeng.2018.09.011.

Chen, J., Mu, T., Goffin, D., Blecker, C., Richard, G., Richel, A., Haubruge, E., 2019b. Application of soy protein isolate and hydrocolloids based mixtures as promising food material in 3D food printing. J. Food Eng. 261, 76–86. https://doi.org/10.1016/j.jfoodeng.2019.03.016.

Chen, Y., Zhang, M., Phuhongsung, P., 2021. 3D printing of protein-based composite fruit and vegetable gel system. LWT - Food Sci. Technol. (Lebensmittel-Wissenschaft -Technol.) 141, 110978. https://doi.org/10.1016/j.lwt.2021.110978.

Costakis, W.J., Rueschhoff, L.M., Diaz-Cano, A.I., Youngblood, J.P., Trice, R.W., 2016. Additive manufacturing of boron carbide via continuous filament direct ink writing of aqueous ceramic suspensions. J. Eur. Ceram. Soc. 36, 3249–3256. https://doi.org/10.1016/j.jeurceramsoc.2016.06.002.

Du, J., Dai, H., Wang, H., Yu, Y., Zhu, H., Fu, Y., Ma, L., Peng, L., Li, L., Wang, Q., Zhang, Y., 2021a. Preparation of high thermal stability gelatin emulsion and its application in 3D printing. Food Hydrocolloids 113, 106536. https://doi.org/10.1016/j.foodhyd.2020.106536.

Du, Y., Zhang, M., Chen, H., 2021b. Effect of whey protein on the 3D printing performance of konjac hybrid gel. LWT - Food Sci. Technol. (Lebensmittel-Wissenschaft -Technol.) 140, 110716. https://doi.org/10.1016/j.lwt.2020.110716.

Godoi, F.C., Prakash, S., Bhandari, B.R., 2016. 3d printing technologies applied for food design: status and prospects. J. Food Eng. 179, 44–54. https://doi.org/10.1016/j.jfoodeng.2016.01.025.

Guo, C., Zhang, M., Devahastin, S., 2021. Improvement of 3D printability of buckwheat starch-pectin system via synergistic Ca2+-microwave pretreatment. Food Hydrocolloids 113, 106483. https://doi.org/10.1016/j.foodhyd.2020.106483.

Lanaro, M., Forrestal, D.P., Scheurer, S., Slinger, D.J., Liao, S., Powell, S.K., Woodruff, M. A., 2017. 3D printing complex chocolate objects: platform design, optimization and evaluation. J. Food Eng. 215, 13–22. https://doi.org/10.1016/j.jfoodeng.2017.06.029.

Le Tohic, C., O'Sullivan, J.J., Drapala, K.P., Chartrin, V., Chan, T., Morrison, A.P., Kerry, J.P., Kelly, A.L., 2018. Effect of 3D printing on the structure and textural properties of processed cheese. J. Food Eng. 220, 56–64. https://doi.org/10.1016/j.jfoodeng.2017.02.003.

Lipton, J.I., 2017. Printable food: the technology and its application in human health. Curr. Opin. Biotechnol. 44, 198–201. https://doi.org/10.1016/j.copbio.2016.11.015.

Liu, Y., Yu, Y., Liu, C., Regenstein, J.M., Liu, X., Zhou, P., 2019a. Rheological and mechanical behavior of milk protein composite gel for extrusion-based 3D food printing. LWT - Food Sci. Technol. (Lebensmittel-Wissenschaft -Technol.) 102, 338–346. https://doi.org/10.1016/j.lwt.2018.12.053.

Liu, Z., Bhandari, B., Prakash, S., Mantihal, S., Zhang, M., 2019b. Linking rheology and printability of a multicomponent gel system of carrageenan-xanthan-starch in extrusion based additive manufacturing. Food Hydrocolloids 87, 413–424. https://doi.org/10.1016/j.foodhyd.2018.08.026.

Liu, Z., Bhandari, B., Prakash, S., Zhang, M., 2018a. Creation of internal structure of mashed potato construct by 3D printing and its textural properties. Food Res. Int. 111, 534–543. https://doi.org/10.1016/j.foodres.2018.05.075.

Liu, Z., Bhandari, B., Zhang, M., 2020a. Incorporation of probiotics (Bifidobacterium animalis subsp. Lactis) into 3D printed mashed potatoes: effects of variables on the viability. Food Res. Int. 128, 108795. https://doi.org/10.1016/j.foodres.2019.108795.

Liu, Z., Chen, H., Zheng, B., Xie, F., Chen, L., 2020b. Understanding the structure and rheological properties of potato starch induced by hot-extrusion 3D printing. Food Hydrocolloids 105, 105812. https://doi.org/10.1016/j.foodhyd.2020.105812.

Liu, Z., Zhang, M., Bhandari, B., 2018b. Effect of gums on the rheological, microstructural and extrusion printing characteristics of mashed potatoes. Int. J. Biol. Macromol. 117, 1179–1187. https://doi.org/10.1016/j.ijbiomac.2018.06.048.

Liu, Z., Zhang, M., Bhandari, B., Yang, C., 2018c. Impact of rheological properties of mashed potatoes on 3D printing. J. Food Eng. 220, 76–82. https://doi.org/10.1016/j.jfoodeng.2017.04.017.

Martínez-Monzó, J., Cárdenas, J., García-Segovia, P., 2019. Effect of temperature on 3D printing of commercial potato puree. Food Biophys. 14, 225–234. https://doi.org/10.1007/s11483-019-09576-0.

Pérez, B., Nykvist, H., Brøgger, A.F., Larsen, M.B., Falkeborg, M.F., 2019. Impact of macronutrients printability and 3D-printer parameters on 3D-food printing: a review. Food Chem. 287, 249–257. https://doi.org/10.1016/j.foodchem.2019.02.090.

Phuhongsung, P., Zhang, M., Devahastin, S., 2020. Investigation on 3D printing ability of soybean protein isolate gels and correlations with their rheological and textural properties via LF-NMR spectroscopic characteristics. LWT - Food Sci. Technol. (Lebensmittel-Wissenschaft -Technol.) 122, 109019. https://doi.org/10.1016/j.lwt.2020.109019.

Pulatsu, E., Su, J.W., Lin, J., Lin, M., 2020. Factors affecting 3D printing and post-processing capacity of cookie dough. Innovat. Food Sci. Emerg. Technol. 61, 102316. https://doi.org/10.1016/j.ifset.2020.102316.

Severini, C., Derossi, A., Ricci, I., Caporizzi, R., Fiore, A., 2018. Printing a blend of fruit and vegetables. New advances on critical variables and shelf life of 3D edible objects. J. Food Eng. 220, 89–100. https://doi.org/10.1016/j.jfoodeng.2017.08.025.

Sun, J., Zhou, W., Huang, D., Fuh, J.Y.H., Hong, G.S., 2015. An overview of 3D printing technologies for food fabrication. Food Bioprocess Technol. 8, 1605–1615. https://doi.org/10.1007/s11947-015-1528-6.

Wang, L., Zhang, M., Bhandari, B., Yang, C., 2018. Investigation on fish surimi gel as promising food material for 3D printing. J. Food Eng. 220, 101–108. https://doi.org/10.1016/j.jfoodeng.2017.02.029.

Yang, F., Zhang, M., Bhandari, B., 2017. Recent development in 3D food printing. Crit. Rev. Food Sci. Nutr. 57, 3145–3153. https://doi.org/10.1080/10408398.2015.1094732.

Yang, F., Zhang, M., Bhandari, B., Liu, Y., 2018. Investigation on lemon juice gel as food material for 3D printing and optimization of printing parameters. LWT - Food Sci. Technol. (Lebensmittel-Wissenschaft -Technol.) 87, 67–76. https://doi.org/10.1016/j.lwt.2017.08.054.

Zeng, X., Chen, H., Chen, L., Zheng, B., 2021. Insights into the relationship between structure and rheological properties of starch gels in hot-extrusion 3D printing. Food Chem. 342, 128362. https://doi.org/10.1016/j.foodchem.2020.128362.

Zhao, Z., Wang, Q., Yan, B., Gao, W., Jiao, X., Huang, J., Zhao, J., Zhang, H., Chen, W., Fan, D., 2020. Synergistic effect of microwave 3D print and transglutaminase on the self-gelation of surimi during printing. Innovat. Food Sci. Emerg. Technol. 67, 102546. https://doi.org/10.1016/j.ifset.2020.102546.

Zhu, S., Stieger, M.A., van der Goot, A.J., Schutyser, M.A.I., 2019. Extrusion-based 3D printing of food pastes: correlating rheological properties with printing behaviour. Innovat. Food Sci. Emerg. Technol. 58, 102214. https://doi.org/10.1016/j.ifset.2019.102214.